# Synthesis and characterization of Gibbsite nanoplatelet brushes by surface-initiated atom transfer radical polymerization

Jianan Zhang <sup>a,b,c</sup> , Jaejun Lee <sup>a</sup> , Zongyu Wang <sup>b</sup> , Jiajun Yan <sup>b</sup> , Zhao Lu <sup>a</sup> , Siyuan Liu <sup>a</sup> , Danli Luo <sup>a</sup> Krzysztof Matyjaszewski* <sup>b</sup> , Michael R. Bockstaller* <sup>a</sup>
<sup>a</sup> Department of Materials Science and Engineering, Carnegie Mellon University, 5000 Forbes Ave., Pittsburgh, PA 15213, United States
<sup>b</sup> Department of Chemistry, Carnegie Mellon University, 4400 Fifth Ave., Pittsburgh, Pennsylvania 15213, United States
<sup>c</sup> School of Chemistry and Chemical Engineering, Anhui University, Hefei 230601, China
Correspondance to: bockstaller@cmu.edu, km3b@andrew.cmu.edu

### **ABSTRACT**

An efficient method for the polymer modification of gibbsite (γ-Al(OH)<sub>3</sub>) nanoplatelet particles with poly(methyl methacrylate) (PMMA) by surface-initiated atom transfer radical polymerization (SI-ATRP) was developed. A newly developed initiator system based on 12-(2-bromoisobutyramido) dodecanoic acid (BiBADA) enable grafting densities in excess of 0.4 nm<sup>-2</sup> with minimal amount of free homopolymer impurities and narrow molecular weight distribution. The gibbsite brush nanoplatelets were shown to organize into transparent films with nacre-like lamellae morphology. A significant increase of the glass transition temperature (as compared to pristine PMMA) was observed and attributed to the increase of steric confinement in planar brush architectures. The applicability of the presented methodology to a wide range of ATRP-compatible chemistries could be a basis for the development of novel functional materials in which properties depend on the directionality of brush nanoplatelet orientation and interaction.

#### 1. Introduction

The grafting of polymer chains to the surface of nanoparticles or colloids constitutes an important process across a wide range of nanomaterial technologies. A well-known example is the application of polymer grafting methods to control of the interactions across particle-polymer interfaces and to facilitate the stable dispersion of particle fillers in polymer matrices. [1-8] More recently, the tethering of polymeric chains also emerged as a viable technique to control interactions between colloidal particles and to enable their assembly into superstructures with novel optical, dielectric, or phononic properties. [9-15] Progress in this novel area of 'one-component polymer hybrid materials' has been promoted by recent advancements in surface-initiated reversible-deactivation radical polymerization (SI-RDRP) techniques that enable high level of control of the architecture of polymer-tethered particles (where the term architecture refers to the degree of polymerization, molecular weight dispersity and grafting density of tethered chains). [16-20] One example is surface-initiated atom transfer radical polymerization (SI-ATRP) that has been demonstrated to facilitate the synthesis of more complex molecular architectures such as bimodal or copolymer brush particles with well-defined characteristics. [21-25]

Key to realize the opportunities of SI-ATRP is the ability to bind initiator moieties to inorganic components. However, while a range of coupling chemistries has been developed for model material systems such as noble metals or silica, the application of SI-ATRP in many dielectrics remains a challenge.[26-28] One example is aluminum hydroxide that has attracted attention as particle fillers to raise the flame retardancy of polymer materials.[29] In the specific case of gibbsite (γ-Al(OH)<sub>3</sub>) additional opportunities arise from the shape anisotropic disc-like morphology of particle fillers, which arises as a consequence of the layered structure of gibbsite and that provides opportunities for the enhancement of mechanical, barrier as well as optical (birefringence) properties of composite materials. In the absence of effective coupling chemistries to surface-modify gibbsite, existing methods have focused on encapsulation strategies to facilitate the polymer-modification of gibbsite

nanoplatelets.[30-32] Poly(methyl methacrylate) (PMMA) encapsulated gibbsite nanoparticles were previously prepared by radical addition–fragmentation chain transfer (RAFT)-based starved feed emulsion polymerization.[4] However, while this report demonstrated the encapsulation of gibbsite nanoplatelets, the properties of the resulting materials and especially their grafting density as well as thermal stability were not investigated. Furthermore, the embedding of gibbsite particles within polymeric capsules significantly limits the attainable inorganic content and thus prevents the formation of liquid-crystal type morphologies.[33]

Recently, 12-(2-bromoisobutyramido) dodecanoic acid (BiBADA) was demonstrated to be a versatile tetherable initiator for SI-ATRP on a variety of metal oxide surfaces. [34] However, this research was limited to polymer grafting from spherical nanoparticles. Polymer tethered non-spherical particles, such as nanoplatelets, provide opportunities for the enhancement of mechanical, barrier as well as optical (birefringence) properties of composite materials arising from the shape anisotropic disc-like morphology of particle fillers. In this contribution, we demonstrate an efficient process for the synthesis of densely PMMA-tethered gibbsite nanoplatelets based on BiBADA initiator system.[34] Using BiBADA as initiator for SI-ATRP facilitated the synthesis of gibbsite-g-PMMA hybrid particles with high grafting density (~0.4 nm<sup>-2</sup>) and inorganic content (~12 wt%) that can be readily organized into one-component hybrid materials with nacre-like morphology and mechanical properties that rival high molecular PMMA.

# 2. Experimental section

## 2.1. Chemicals

Aluminum isopropoxide (AIP,  $\geq$  98 %, Aldrich), aluminum sec-butoxide (ASB, 97 %, Aldrich), and hydrochloric acid (HCl, 37 %, Acros) were used as received. Methyl methacrylate (MMA) was purified by passing through a basic alumina column. Copper (I) chloride was prepared by reduction of CuCl<sub>2</sub> (aq) solution using an aqueous solution of sodium sulfite and then sequentially filtered, washed

with methanol, dried, and stored under vacuum before use. Copper (I) chloride (CuCl, Alfa, 99.999 %), 4,4  $^{\prime}$  -dinonyl-2,2  $^{\prime}$  -bipyridine (dNbpy) (Aldrich, 99 %), and N, N, N  $^{\prime}$  , N", N"-pentamethyldiethylene triamine (PMDETA) (Aldrich, 99 %) were used as received. All other chemicals and solvents were obtained from Aldrich and Acros Organics. Milli-Q water with a resistivity higher than 18.2 M $\Omega$  was used in all preparations.

## 2.2. Synthesis of gibbsite nanoplatelets

Gibbsite nanoplatelets (γ-Al(OH)<sub>3</sub>) were synthesized from AIP and ASB according to the reported methods.[32, 35] In a typical experiment, 0.08 mol/L ASB and 0.08 mol/L AIP were dissolved in 1.5 L of deionized water which was acidified by 0.09 mol/L HCl. After mechanically stirring for 10 days, the turbid mixture was heated in a polypropylene bottle in a water bath at 85 °C for 3 days and then dialyzed against deionized water for several days until the conductivity dropped to 20 μS/cm. Finally, the colloidal dispersion was centrifuged to remove the small gibbsite particles before further characterization and use.

# 2.3. Preparation of gibbsite-g-polymer particle brushes by SI-ATRP

The 12-(2-bromoisobutyramido) dodecanoic acid (BiBADA) was synthesized according to the recent report.[34] The as-prepared gibbsite nanoplatelets were surface modified by BiBADA. The general procedure of surface modification was as follows. A measured amount of BiBADA (five molecules per nm² of the nanoplatelet surface were added in a 0.05 g/mL dispersion of gibbsite nanoplatelets in tetrahydrofuran (THF). The mixture was sonicated in a sonication bath for 24 h to ensure sufficient separation of nanoplatelet aggregates and contact of the exposed surfaces with BiBADA. After surface modification, the stability of nanoplatelet dispersions in THF was significantly improved. The surface modified gibbsite nanoplatelets were purified by centrifugation for 3 times in a sonication-centrifuge (4000 G) cycle to remove the surplus BiBADA. The polymer grafting from surface modified gibbsite nanoplatelets was carried out by normal ATRP. A typical reaction condition follows [Gibbsite-

Br]<sub>0</sub>/[MMA]<sub>0</sub>/[CuCl<sub>2</sub>]<sub>0</sub>/[CuCl]<sub>0</sub>/[dNbpy]<sub>0</sub> = 1:1000:0.1:0.9:2.0; 35 vol % anisole. The mixture was bubbled with nitrogen for 30 min and then flash-frozen in liquid nitrogen before CuCl was added. The frozen mixture was purged with nitrogen for another 5 min, and then warmed to room temperature and placed in an oil bath heated to 60 °C to initiate polymerization. The polymerization was stopped by exposing the catalyst to oxygenated THF after cooling under continuous stirring. The product was precipitated by adding the reaction mixture to methanol and the solid was filtered and washed with methanol. The preparation of silica-*g*-PMMA was performed using SI-ATRP according to previously published procedures.[10, 36]

### 2.4. Characterization

Molecular weight and molecular weight distribution of surface-grafted chains were determined by gel permeation chromatography (GPC) after etching process. The GPC was conducted with a Waters 515 pump and Waters 410 differential refractometer using PSS columns (Styrogel 10<sup>5</sup>, 10<sup>3</sup>, 10<sup>2</sup> Å) in THF as an eluent (35 °C, flow rate of 1 mL/min). Linear PMMA standards were used for GPC calibration. Differential scanning calorimetry (DSC) was performed on a Perkin-Elmer Diamond DSC with a heating rate of 20 °C/min under nitrogen flow (20 mL/min). The thermogravimetric analysis (TGA) was conducted using a TA Instrument TGA 2950 and the data was analyzed with TA Universal Analysis. The heating procedure involved four steps: (1) jump to 120 °C; (2) hold at 120 °C for 10 min; (3) ramp at a rate of 20 °C/min to 800 °C; (4) hold for 5 min. The TGA plots were normalized to the total weight after holding at 120 °C. The graft density of hybrid particles was calculated from the obtained TGA results. The hydrodynamic size distribution of the polymer-grafted nanoparticles was determined by a Malvern Zetasizer Nano ZS particle size analyzer. Scanning electron microscopy (SEM) analysis was conducted using a Hitachi 2460N scanning electron microscope. The specimens were attached to SEM stubs and coated with gold using a Pelco SC-6 sputter coater prior to imaging. The morphologies of gibbsite-g-PMMA particles were studied with the aid of transmission electron microscopy (TEM) (Hitachi H-7100 electron microscope operating at 200 kV). To visualize and detect the microstructure of gibbsite-g-PMMA film, ultrathin sections (70-90 nm thick) of the film were cut with a LKB ultratome 8800 ultramicrotome and transferred on copper grids for TEM characterization.

### 2.5. Nanoindentation

Elastic modulus was measured via nanoindentation. Measurements were conducted using an MTS Nanoindenter XP with a Berkovich tip under that displacement was controlled to 200 nm. The displacement rate during indenting on samples was 5 nm s<sup>-1</sup> to maximum load, and the indenter held constant load for 10 seconds at peak. Experimental data were acquired from 25 (5×5) indentations on each sample under an allowable drift rate of 0.05 nm/s. The error of the measurements was calculated as experimental error.

### 3. Results and Discussion

## 3.1. Morphology investigation of gibbsite nanoplatelets and gibbsite nanoplatelet brushes

Gibbsite nanoplatelets were synthesized from aluminum alkoxides in an acidic aqueous solution at 85 °C, according to the method reported by Wierenga et al.[32, 35] To purify gibbsite nanoplatelets, a multiple centrifugation-redispersion process was adopted to remove unreacted agents and small particles. Representative electron images of the as-synthesized gibbsite nanoplatelets are shown in **Fig.**1. The figure reveals that particles were of uniform hexagonal shape with a diameter of  $175 \pm 25$  nm.[37] The  $\zeta$ -potential of the particles was determined to be  $+49.5\pm1.2$  mV in good agreement with previous results.[38] The high surface charge renders nanoplatelet dispersions in aqueous and alcoholic solvents stable without detectable aggregation. The pristine gibbsite nanoplatelets were well dispersed in water as shown in inset of Fig. 1a.

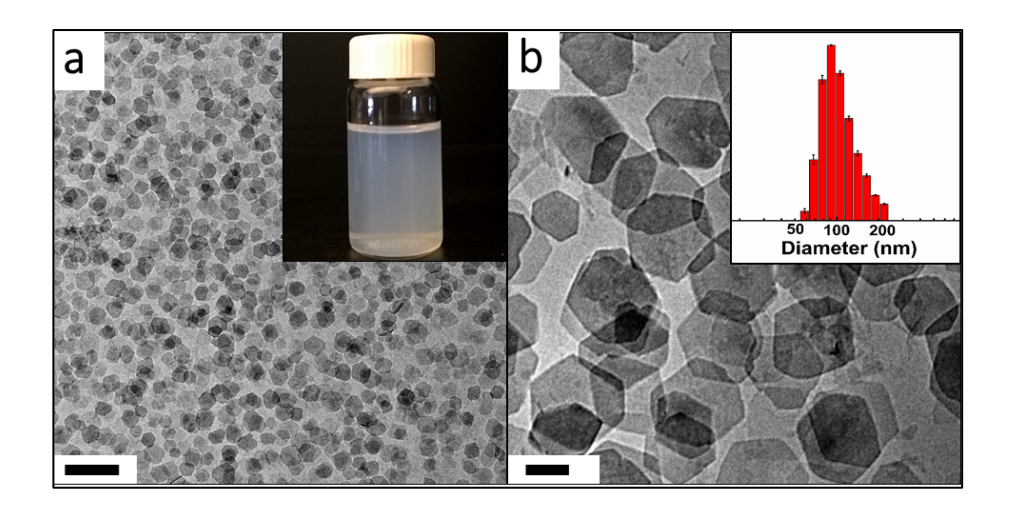


**Fig. 1.** Representative transmission electron micrograph of gibbsite nanoplatelets at different magnifications. Scale bars are 500 nm (a) and 100 nm (b). Inset of Fig. 1a shows the photograph of pristine gibbsite dispersion in water. Inset of Fig. 1b shows the number weighted size distribution of gibbsite nanoplatelets as determined by dynamic light scattering (DLS) in aqueous solution.

The positive net charge of platelets facilitates the application of negatively charged initiators such as BiBADA that are expected to form strong bonds with the gibbsite particles. The initiator immobilization was performed under sonication to facilitate coupling reaction by addition of BiBADA into nanoplatelets dispersion. The resulting initiator-capped gibbsite particles formed stable dispersions in unpolar organic solvents. SI-ATRP was subsequently applied to grow PMMA from the gibbsite surface, following previously published procedures.[34] In the first step, the colloidal dispersion of gibbsite nanoplatelets was purified by centrifugation and dispersed in THF. After the addition of the tetherable initiator (BiBADA), the mixture was sonicated in a sonication bath for 24 h and the surface modified gibbsite nanoplatelets were obtained after purification by centrifugation for 3 times. As mentioned above, the BiBADA systems was recently found to be a versatile initiator for a wide range of metal oxide chemistries. Binding between BiBADA and the metal oxide presumably occurs via ionic charge interaction (see illustration in Fig. 2a). This is because the pKa of oleic acid is approximately 10.2 and hence BiBADA is expected to be fully ionized at the working pH. We note that the binding mechanism is expected to be analogous to deprotonated oleic acid that is one of the most commonly used ligands for stabilization of metal oxide nanoparticles.[39, 40] The polymer-

grafted gibbsite nanoplatelets were subsequently prepared by SI-ATRP. The process is illustrated in **Fig. 2a**. Two systems were synthesized with degrees of polymerization of PMMA of 610 and 982, respectively. The degree of polymerization of tethered chains was determined by GPC analysis after etching of the particle core using 0.5 M HCl (**Fig. 2b**). The narrow molecular weight distributions of the tethered polymer chains (D = 1.1) demonstrated the well-controlled polymer grafting by SI-ATRP. **Fig. 2c**, **d** show representative electron micrographs of nanoplatelet brushes along with the respective particle size distribution as determined by DLS. Partial aggregation that is observed in the electron micrograph is caused by the drying of solutions (presumably through the action of capillary interactions). The good dispersion behavior in solution is confirmed by DLS of platelet brush solutions as revealed by the near single exponential time correlation function shown in inset of Fig. 2d.

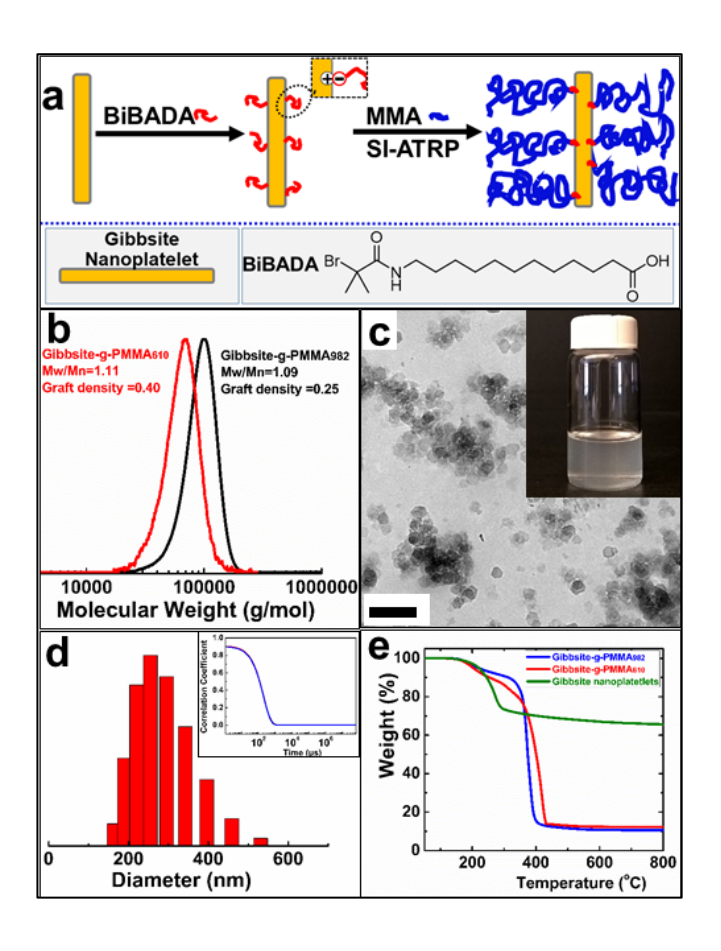


**Fig. 2.** (a) Scheme of the synthesis of gibbsite-*g*-polymer nanocomposite by SI-ATRP. The purified gibbsite nanoplatelets were mixed with BiBADA to obtain initiator modified gibbsite nanoplatelets. After polymer grafting gibbsite nanoplatelet brushes were fabricated by SI-ATRP. (b) GPC traces of the tethered PMMA chains after etching away the corresponding gibbsite cores. (c) Representative transmission electron micrograph of gibbsite-*g*-PMMA<sub>610</sub> (scale bar is 500 nm). Partial aggregation of

particles occurs during the drying of films. (d) DLS of gibbsite-g-PMMA<sub>610</sub> brush. (e) TGA analysis of gibbsite-g-PMMA<sub>610</sub>, and gibbsite-g-PMMA<sub>982</sub>. Inset in Fig. 2c shows the photograph of nanoplatelet brush solution in THF and inset in Fig. 2d shows the time correlation function obtained by DLS.

The thermal degradation behavior of neat gibbsite and gibbsite-g-PMMA nanocomposites with different degrees of polymerization were studied by TGA, by heating from room temperature to 800 °C at a heating rate of 10 °C/min under air atmosphere. The results are shown in **Fig. 2e**. For comparison, silica-g-PMMA with similar inorganic content was selected to investigate its thermal stability (**Fig. S1**).[10] The weight fraction of PMMA nanocomposite film is 87.8 wt% for gibbsite-g-PMMA<sub>610</sub> and 89.4 wt% for gibbsite-g-PMMA<sub>982</sub>, which are similar to that of 15 nm silica-g-PMMA<sub>350</sub>. By calculation from TGA results, the graft density of gibbsite nanocomposites was  $\sigma = 0.40$  and 0.25 nm<sup>-2</sup> for gibbsite-g-PMMA<sub>610</sub> and gibbsite-g-PMMA<sub>982</sub>, respectively.

For gibbsite nanoplatelets, an apparent thermal degradation process occurred prior to ~270 °C that corresponded to the decomposition reaction of gibbsite 2 Al(OH)<sub>3</sub> $\rightarrow$ Al<sub>2</sub>O<sub>3</sub> + 3 H<sub>2</sub>O.[35] The residue was solely Al<sub>2</sub>O<sub>3</sub> and the mass percentage was about 65.5 wt%. This value was consistent with the theoretical value of 65.4 wt%, calculated from gibbsite decomposition according to the above reaction. Both gibbsite-*g*-PMMA nanocomposites had higher 100 % weight loss temperatures than that of silica-*g*-PMMA<sub>350</sub> (**Fig. S1**). The much lower  $T_{\text{onset}}$  (*i.e.* temperature at 5 % weight loss) of gibbsite-*g*-PMMA nanocomposites was due to the decomposition of gibbsite nanoplatelets (**Table S1**). This beneficial effect is rationalized as a consequence of the increased barrier properties due to the presence of gibbsite nanoplatelets, which restricts the transmission of heat and thus limits the continuous decomposition of polymers.

## 3.2. Structural investigation of gibbsite-g-polymer nanocomposite film

Freestanding nanocomposite films were fabricated by solution casting of gibbsite-g-PMMA nanoplatelets from 10 wt% toluene solution. **Fig. 3** depicts the structure of a free standing film of gibbsite-g-PMMA<sub>982</sub> of 0.3 mm thickness.

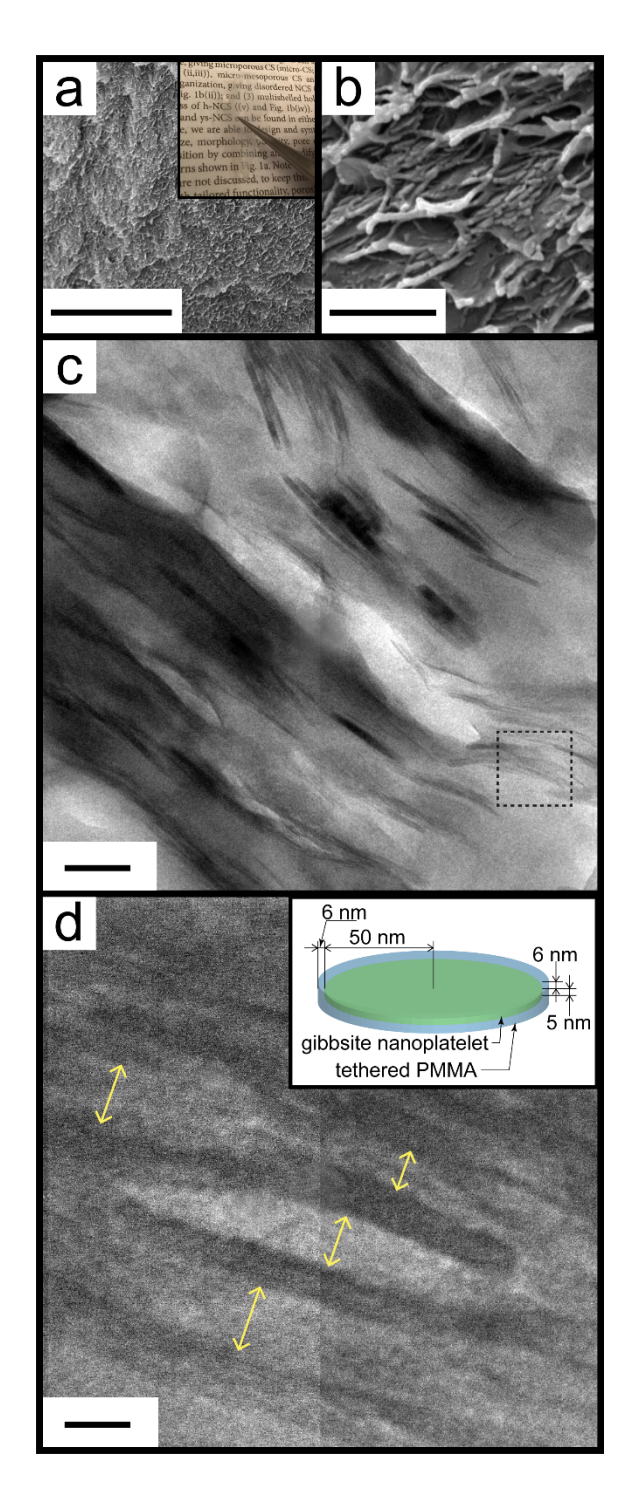


**Fig. 3.** Microstructure of gibbsite-*g*-PMMA<sub>982</sub> nanocomposites. (a) Top view (scale bar is 20 μm) and (b) cross-sectional view of SEM images of gibbsite-*g*-PMMA<sub>982</sub> nanocomposite film (scale bar is 1 μm). (c) The cross-sectional TEM images of gibbsite-*g*-PMMA<sub>982</sub> nanocomposite films (scale bar is 100 nm), and (d) partially enlarged cross-sectional view of (c) (scale bar is 10 nm). Particle density fluctuations that are observed in the micrograph are caused by mechanical distortion of the film during microsectioning. The inset in (a) shows a photograph of the transparent free-standing nanocomposite film of gibbsite-*g*-PMMA<sub>982</sub> sample. The inset in (d) depicts a schematic illustration of the model assumption for estimation of the grafting density from the TEM micrograph shown in the main figure.

The optical transparency of the film (Fig. 3a) confirms its uniform microstructure that is characteristic of one-component particle brush hybrid materials. Scanning (Fig. 3b) and transmission (Figs. 3c, d) electron imaging of microsectioned film samples reveal an anisotropic nacre-like microstructure that is formed by stacking of nanoplatelet brushes. The liquid-crystalline type order of 'nanoplatelet lamellae' that is observed in Figs. 3c and 3d is consistent with the expected shape anisotropy  $a/b \sim 5$ of polymer-tethered nanoplatelets (where a and b represent the diameter and thickness of brush platelets, respectively). Note that the micrograph in Fig. 3c also reveals non-uniformity in the distribution of nanoplatelets across the imaged film. To better understand the origin of the apparent heterogeneity (i.e. mechanical shear distortion of platelet film during microsectioning or the presence of untethered PMMA), the grafting density of nanoplatelet brushes was independently estimated by analysis of electron micrographs. Specifically, the micrograph of gibbsite-g-PMMA982 lamellar structures (Fig. 3d) reveals a lamellar spacing of r = 5 nm. Assuming a constant mass density of the PMMA layer ( $\rho = 1.18$  g/mL) the grafting density can be estimated as  $\sigma_{\text{TEM}} = n_{\text{PMMA}}/A \approx$  $V_{\rm PMMA} r_{\rm PMMA} (M_{\rm PMMA} N_{\rm Av})^{-1} / (2\pi R^2 + 2\pi Rt)$  where R = 50 nm and t = 5 nm represent the average radius and thickness of nanoplatelets and  $V_{PMMA}$  is the volume of tethered PMMA deduced from the geometry shown in the inset of Fig. 3d.[41] The excellent agreement between  $\sigma_{TEM} = 0.24$  nm<sup>-2</sup> and the result from TGA analysis ( $\sigma_{TGA} = 0.25 \text{ nm}^{-2}$ ) suggests that the heterogeneity observed in **Fig. 3c** is indeed caused by mechanical deformation (shearing) of samples during the sectioning process rather than the presence of free homopolymer impurities.

To evaluate the effect of the nacre-like microstructures on the mechanical properties of gibbsite-hybrid materials, the elastic moduli of gibbsite-g-PMMA<sub>610</sub> and gibbsite-g-PMMA<sub>982</sub> (as well as the respective reference homopolymers) films were evaluated using nanoindentation. The latter has emerged as a versatile technique to evaluate the mechanical properties of particulate films.[11, 13] Albeit indentation cannot be considered to be an 'absolute technique' (since the deduction of physical properties requires the assumption of idealized material behavior), it has been shown to be reliable in

determining differences and trends in material behavior. Force-displacement curves were measured at a displacement rate of 5 nm s<sup>-1</sup> to the maximum load followed by constant load indentation for 20 seconds before unloading since previous research has shown viscoelastic effects under these conditions to be negligible [11, 13]. Representative force-displacement data along with an AFM image of a typical indent are shown in **Fig. 4.** 

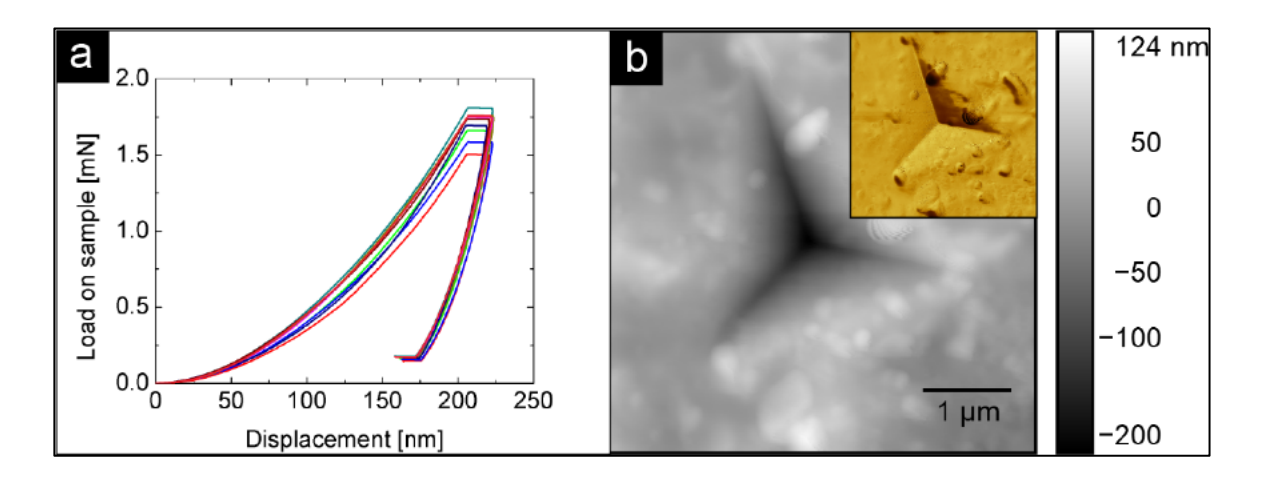


**Fig. 4.** Representative data obtained by nanoindentation of gibbsite-*g*-PMMA<sub>610</sub>. Panel a shows force displacement curves measured at 5 nm s<sup>-1</sup>. Panel b shows representative AFM height image of indent. Inset depicts corresponding phase image.

The indentation results for hardness H and modulus E are presented in **Table 1** that also presents a comparison with PMMA-tethered spherical silica nanospheres (diameter  $\sim 15$  nm) with similar inorganic content to discern the role of geometric shape on particle brush interactions. Synthesis and characterization of silica-g-PMMA brush particles followed analogous procedures as previously reported.[11, 42]

**Table 1.** Summary of material characteristics and mechanical properties of gibbsite- and silica brush particle systems.

sample ID	N	Đ	σ	$ extit{f}_{inorg}$	φ <sub>inorg</sub>	Ε	Н
			/nm <sup>-2</sup>	wt%	vol%	/GPa	/GPa
silica-g-PMMA <sub>637</sub>	637	1.12	0.19	11.5	7.0	1.43 ± 0.32	0.25 ± 0.07
silica-g-PMMA <sub>309</sub>	309	1.13	0.71	13.1	8.1	1.65 ± 0.16	0.30 ± 0.05
gibbsite-g-PMMA <sub>610</sub>	610	1.11	0.40	12.1	6.8	1.22 ± 0.55	0.16 ± 0.14
gibbsite-g-PMMA <sub>982</sub>	982	1.09	0.25	10.6	5.8	0.83 ± 0.10	0.03 ± 0.01

Note that both brush systems exhibit similar inorganic volume fraction and hence the results should primarily reflect the influence of particle shape and degree of polymerization of tethered chains. **Table**1 reveals several pertinent features. First, in both systems the elastic modulus is found to increase with inorganic content. This agrees with the expectation that the stiffness of the total system increases with the concentration of the stiffer component. Interestingly, the data also suggests that gibbsite-brush systems exhibit a reduced elastic modulus as compared to the spherical brush analogs (although the rather significant error bar in case of gibbsite-g-PMMA<sub>610</sub> renders a conclusion somewhat ambiguous). We speculate that this softer response of platelet brushes is attributable to the increased geometric confinement in planar brush systems that will alter the conformation of tethered chains and hence the interaction between brush particles.

## 3.3. Thermal properties of gibbsite-g-polymer nanocomposite film

The change of chain conformations due to steric confinement in brush architectures is known to alter the relaxation behavior of surface-tethered chains and hence the polymer's glass transition temperature  $(T_g)$ .[40] To evaluate the glass transition temperature DSC analysis was carried out on self-assembled one-component gibbsite-g-PMMA hybrid materials. As shown in **Fig. 5**, in the first cycle of both gibbsite brushes, the peak at 137 °C corresponded to the dehydration of gibbsite  $(\gamma$ -Al(OH)<sub>3</sub>), as

observed in the above TGA analysis. Upon conditioning of films (3<sup>rd</sup> cycle) the glass transition temperature of PMMA the  $T_g$  of gibbsite-g-PMMA<sub>610</sub> brush platelets was determined as  $T_g = 126.3$  °C.

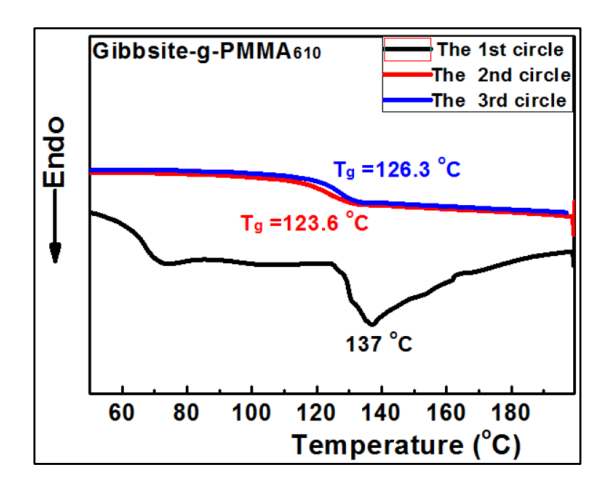


**Fig. 5.** DSC traces of gibbsite-*g*-PMMA<sub>610</sub> nanocomposites. The distinctive change in heat capacity in the first heating circle is attributed to gibbsite dehydration.

The remarkable increase of the glass transition temperature as compared to pristine PMMA of similar molecular weight ( $T_{\rm g,PMMA} \sim 105~{\rm ^{\circ}C}$ ) is interpreted as a consequence of the increased steric hindrance in platelet brushes that constrains chain relaxation. This is in contrast to spherical brush particles that display only minor increased values of  $T_{\rm g}$  as compared to linear polymer reference systems.[43] The increase in glass temperatures therefore supports the lack of increase in mechanical strength of the present brush nanoplatelet materials (**Table S1**), since increased excluded volume interactions (due to the constraining effect of the planar surface) would also be expected to reduce chain entanglement and thus resistance to mechanical deformation.[13]

### 4. Conclusions

A facile methodology for the synthesis of densely PMMA-tethered gibbsite nanoplatelets using SI-ATRP was developed. Harnessing strong coupling interactions between positively charged gibbsite and the dodecanoic acid-based initiator BiBADA a grafting density of ~0.4 nm<sup>-2</sup> was demonstrated. Good agreement between the platelet brush compositions based on thermogravimetric and

morphological analysis suggest that only small amounts of free homopolymer are being formed during

the synthesis. The structural uniformity of nanoplatelet brush particles gave rise to nacre-like lamellae

microstructures of films. Despite the structural similarity to 'conventional' spherical brush particle

systems several distinctive features are observed for nanoplatelet brushes. For example, a pronounced

increase of the glass transition temperature as compared to untethered polymer is observed and

attributed to the more pronounced steric confinement of chains on planar surfaces. The presented

methodology should be applicable to a wide range of ATRP-compatible chemistries and hence could

be the basis for the development of novel functional materials based on nanoplatelet brush materials.

To accomplish this goal future research will have to develop better understanding about the

relationship between the molecular architecture of platelet-brush materials and brush nanoplatelet

interactions as well as methodologies for the preparation of microstructure with controlled platelet

orientation.

Acknowledgements

The authors acknowledge funding by the National Science Foundation via grants CMMI-1663305,

DMR 15001324, as well as National Science Centre, Poland (via Grant UMO-2014/14/A/ST5/00204).

J.Z. acknowledges a scholarship from the China Scholarship Council (CSC).

**ORCID** 

Michael R. Bockstaller: 0000-0001-9046-9539

Krzysztof Matyjaszewski: 0000-0003-1960-3402

Jiajun Yan: 0000-0003-3286-3268

Jianan Zhang: 0000-0003-3195-9882

16

#### References

- [1] C. Mahoney, C.M. Hui, S. Majumdar, Z. Wang, J.A. Malen, M.N. Tchoul, K. Matyjaszewski, M.R. Bockstaller, Enhancing thermal transport in nanocomposites by polymer-graft modification of particle fillers, Polymer 93 (2016) 72-77.
- [2] A. Dang, S. Ojha, C.M. Hui, C. Mahoney, K. Matyjaszewski, M.R. Bockstaller, High-transparency polymer nanocomposites enabled by polymer-graft modification of particle fillers, Langmuir 30(48) (2014) 14434-42.
- [3] S. Ojha, A. Dang, C.M. Hui, C. Mahoney, K. Matyjaszewski, M.R. Bockstaller, Strategies for the synthesis of thermoplastic polymer nanocomposite materials with high inorganic filling fraction, Langmuir 29(28) (2013) 8989-96.
- [4] S.I. Ali, J.P. Heuts, B.S. Hawkett, A.M. van Herk, Polymer encapsulated gibbsite nanoparticles: efficient preparation of anisotropic composite latex particles by RAFT-based starved feed emulsion polymerization, Langmuir 25(18) (2009) 10523-33.
- [5] H. Oh, P.F. Green, Polymer chain dynamics and glass transition in athermal polymer/nanoparticle mixtures, Nat. Mater. 8(2) (2009) 139-43.
- [6] S.K. Kumar, N. Jouault, B. Benicewicz, T. Neely, Nanocomposites with polymer grafted nanoparticles, Macromolecules 46(9) (2013) 3199-3214.
- [7] P. Akcora, H. Liu, S.K. Kumar, J. Moll, Y. Li, B.C. Benicewicz, L.S. Schadler, D. Acehan, A.Z. Panagiotopoulos, V. Pryamitsyn, V. Ganesan, J. Ilavsky, P. Thiyagarajan, R.H. Colby, J.F. Douglas, Anisotropic self-assembly of spherical polymer-grafted nanoparticles, Nat. Mater. 8(4) (2009) 354-9. [8] R. Krishnamoorti, R.A. Vaia, Polymer nanocomposites, J. Polym. Sci., Part B: Polym. Phys. 45(24) (2007) 3252-3256.
- [9] E. Alonso-Redondo, M. Schmitt, Z. Urbach, C. Hui, R. Sainidou, P. Rembert, K. Matyjaszewski, M. Bockstaller, G. Fytas, A new class of tunable hypersonic phononic crystals based on polymertethered colloids, Nat. Commun. 6 (2015) 8309.
- [10] M. Schmitt, J. Zhang, J. Lee, B. Lee, X. Ning, R. Zhang, A. Karim, R.F. Davis, K. Matyjaszewski, M.R. Bockstaller, Polymer ligand-induced autonomous sorting and reversible phase separation in binary particle blends, Sci. Adv. 2(12) (2016) e1601484.
- [11] J. Choi, C.M. Hui, J. Pietrasik, H. Dong, K. Matyjaszewski, M.R. Bockstaller, Toughening fragile matter: mechanical properties of particle solids assembled from polymer-grafted hybrid particles synthesized by ATRP, Soft Matter 8(15) (2012) 4072-4082.
- [12] C.A. Grabowski, H. Koerner, J.S. Meth, A. Dang, C.M. Hui, K. Matyjaszewski, M.R. Bockstaller, M.F. Durstock, R.A. Vaia, Performance of dielectric nanocomposites: matrix-free, hairy nanoparticle assemblies and amorphous polymer-nanoparticle blends, ACS Appl. Mater. Interfaces 6(23) (2014) 21500-9.
- [13] M. Schmitt, J. Choi, C.M. Hui, B. Chen, E. Korkmaz, J. Yan, S. Margel, O.B. Ozdoganlar, K. Matyjaszewski, M.R. Bockstaller, Processing fragile matter: effect of polymer graft modification on the mechanical properties and processibility of (nano-) particulate solids, Soft Matter 12(15) (2016) 3527-37.
- [14] M.A. Boles, M. Engel, D.V. Talapin, Self-Assembly of Colloidal Nanocrystals: From Intricate Structures to Functional Materials, Chem. Rev. 116(18) (2016) 11220-89.
- [15] L. Wang, M. Cole, J. Li, Y. Zheng, Y.P. Chen, K.P. Miller, A.W. Decho, B.C. Benicewicz, Polymer grafted recyclable magnetic nanoparticles, Polym. Chem. 6(2) (2015) 248-255.
- [16] R. Barbey, L. Lavanant, D. Paripovic, N. Schuwer, C. Sugnaux, S. Tugulu, H.A. Klok, Polymer brushes via surface-initiated controlled radical polymerization: synthesis, characterization, properties, and applications, Chem. Rev. 109(11) (2009) 5437-527.
- [17] J.-S. Wang, K. Matyjaszewski, Controlled/"living" radical polymerization. atom transfer radical polymerization in the presence of transition-metal complexes, J. Am. Chem. Soc. 117(20) (1995) 5614-5615.

- [18] W.A. Braunecker, K. Matyjaszewski, Controlled/living radical polymerization: Features, developments, and perspectives, Prog. Polym. Sci. 32(1) (2007) 93-146.
- [19] K. Matyjaszewski, Atom transfer radical polymerization (ATRP): current status and future perspectives, Macromolecules 45(10) (2012) 4015-4039.
- [20] J.O. Zoppe, N.C. Ataman, P. Mocny, J. Wang, J. Moraes, H.-A. Klok, Surface-Initiated Controlled Radical Polymerization: State-of-the-Art, Opportunities, and Challenges in Surface and Interface Engineering with Polymer Brushes, Chem. Rev 117(3) (2017) 1105-1318.
- [21] C.M. Hui, J. Pietrasik, M. Schmitt, C. Mahoney, J. Choi, M.R. Bockstaller, K. Matyjaszewski, Surface-initiated polymerization as an enabling tool for multifunctional (nano-) engineered hybrid materials, Chem. Mater. 26(1) (2013) 745-762.
- [22] K. Matyjaszewski, N.V. Tsarevsky, Macromolecular engineering by atom transfer radical polymerization, J. Am. Chem. Soc. 136(18) (2014) 6513-33.
- [23] J. Yan, T. Kristufek, M. Schmitt, Z. Wang, G. Xie, A. Dang, C.M. Hui, J. Pietrasik, M.R. Bockstaller, K. Matyjaszewski, Matrix-free Particle Brush System with Bimodal Molecular Weight Distribution Prepared by SI-ATRP, Macromolecules 48(22) (2015) 8208-8218.
- [24] A. Khabibullin, E. Mastan, K. Matyjaszewski, S. Zhu, Surface-initiated atom transfer radical polymerization, Controlled Radical Polymerization at and from Solid Surfaces, Springer2015, pp. 29-76.
- [25] W.-L. Chen, R. Cordero, H. Tran, C.K. Ober, 50th Anniversary Perspective: Polymer Brushes: Novel Surfaces for Future Materials, Macromolecules (2017).
- [26] K. Ohno, K. Koh, Y. Tsujii, T. Fukuda, Fabrication of ordered arrays of gold nanoparticles coated with high-density polymer brushes, Angew. Chem. Int. Ed. Engl. 42(24) (2003) 2751-4.
- [27] E. Marutani, S. Yamamoto, T. Ninjbadgar, Y. Tsujii, T. Fukuda, M. Takano, Surface-initiated atom transfer radical polymerization of methyl methacrylate on magnetite nanoparticles, Polymer 45(7) (2004) 2231-2235.
- [28] K. Ohno, T. Morinaga, K. Koh, Y. Tsujii, T. Fukuda, Synthesis of monodisperse silica particles coated with well-defined, high-density polymer brushes by surface-initiated atom transfer radical polymerization, Macromolecules 38(6) (2005) 2137-2142.
- [29] A. Mousa, J. Karger-Kocsis, Rheological and thermodynamical behavior of styrene/butadiene rubber-organoclay nanocomposites, Macromol. Mater. Eng. 286(4) (2001) 260-266.
- [30] O.P. Loiko, A.B. Spoelstra, A.M. van Herk, J. Meuldijk, J.P. Heuts, An ATRP-based approach towards water-borne anisotropic polymer–Gibbsite nanocomposites, Polym. Chem. 7(20) (2016) 3383-3391.
- [31] D.J. Voorn, W. Ming, A.M. van Herk, P.H. Bomans, P.M. Frederik, P. Gasemjit, D. Johanssmann, Controlled heterocoagulation of platelets and spheres, Langmuir 21(15) (2005) 6950-6.
- [32] J. Cao, S. Mei, H. Jia, A. Ott, M. Ballauff, Y. Lu, In Situ Synthesis of Catalytic Active Au Nanoparticles onto Gibbsite-Polydopamine Core-Shell Nanoplates, Langmuir 31(34) (2015) 9483-91.
- [33] A. Aijaz, N. Fujiwara, Q. Xu, From metal—organic framework to nitrogen-decorated nanoporous carbons: high CO2 uptake and efficient catalytic oxygen reduction, J. Am. Chem. Soc. 136(19) (2014) 6790-6793.
- [34] J. Yan, X. Pan, Z. Wang, Z. Lu, Y. Wang, L. Liu, J. Zhang, C. Ho, M.R. Bockstaller, K. Matyjaszewski, A Fatty Acid-Inspired Tetherable Initiator for Surface-Initiated Atom Transfer Radical Polymerization, Chem. Mater. 29(11) (2017) 4963-4969.
- [35] A.M. Wierenga, T.A. Lenstra, A.P. Philipse, Aqueous dispersions of colloidal gibbsite platelets: synthesis, characterisation and intrinsic viscosity measurements, Colloids and Surfaces A: Physicochemical and Engineering Aspects 134(3) (1998) 359-371.
- [36] J. Pyun, K. Matyjaszewski, Synthesis of nanocomposite organic/inorganic hybrid materials using controlled/"living" radical polymerization, Chem. Mater. 13(10) (2001) 3436-3448.
- [37] S. Liu, J. Zhang, N. Wang, W. Liu, C. Zhang, D. Sun, Liquid-crystalline phases of colloidal dispersions of layered double hydroxides, Chem. Mater. 15(17) (2003) 3240-3241.

- [38] T.-H. Lin, W.-H. Huang, I.-K. Jun, P. Jiang, Bioinspired assembly of colloidal nanoplatelets by electric field, Chem. Mater. 21(10) (2009) 2039-2044.
- [39] L. Zhang, R. He, H.-C. Gu, Oleic acid coating on the monodisperse magnetite nanoparticles, Appl. Surf. Sci. 253(5) (2006) 2611-2617.
- [40] N. Wu, L. Fu, M. Su, M. Aslam, K.C. Wong, V.P. Dravid, Interaction of fatty acid monolayers with cobalt nanoparticles, Nano Lett. 4(2) (2004) 383-386.
- [41] J. Brandrup, E.H. Immergut, E.A. Grulke, A. Abe, D.R. Bloch, Polymer handbook, Wiley New York etc1989.
- [42] J. Choi, H. Dong, K. Matyjaszewski, M.R. Bockstaller, Flexible particle array structures by controlling polymer graft architecture, J. Am. Chem. Soc. 132(36) (2010) 12537-9.
- [43] M. Schmitt, C.M. Hui, Z. Urbach, J. Yan, K. Matyjaszewski, M.R. Bockstaller, Tailoring structure formation and mechanical properties of particle brush solids via homopolymer addition, Faraday Discuss. 186 (2016) 17-30.

**ToC** 

